Biology of Reproduction, 2020, 102(6), 1234–1247
doi:10.1093/biolre/ioaa024
Research Article
Advance Access Publication Date: 26 February 2020

OXFORD

Research Article

Knockout of mouse receptor accessory protein 6 leads to sperm function and morphology defects†

Darius J. Devlin[1,2,‡], Smriti Agrawal Zaneveld[3,4,‡], Kaori Nozawa[2,5], Xiao Han[3,4,7], Abigail R. Moye[6], Qingnan Liang[3,4,6], Jacob Michael Harnish[4], Martin M. Matzuk[2,4,5,*] and Rui Chen[3,4,*]

[1]Interdepartmental Program in Translational Biology & Molecular Medicine, Baylor College of Medicine, Houston, TX, USA, [2]Department of Pathology & Immunology, Baylor College of Medicine, Houston, TX, USA, [3]Human Genome Sequencing Center, Baylor College of Medicine, Houston, TX, USA, [4]Department of Molecular and Human Genetics, Baylor College of Medicine, Houston, TX, USA, [5]Center for Drug Discovery, Baylor College of Medicine, Houston, TX, USA, [6]Department of Biochemistry and Molecular Biology, Baylor College of Medicine, Houston, TX, USA, and [7]Reproductive Medical Center, People's Hospital of Zhengzhou University, Zhengzhou, China

***Correspondence**: Center for Drug Discovery and Department of Pathology & Immunology, Baylor College of Medicine, One Baylor Plaza, Houston, TX 77030, USA. Tel: (713) 798-6451, (713) 798-5838; E-mail: mmatzuk@bcm.edu (Martin M. Matzuk); Human Genome Sequencing Center and Department of Molecular and Human Genetics, Baylor College of Medicine, One Baylor Plaza, Houston, TX 77030, USA. Tel: (713) 798-5194, (713) 798-5741; E-mail: ruichen@bcm.edu (Rui Chen)

† **Grant Support**: Eunice Kennedy Shriver National Institute of Child Health and Human Development (R01HD088412 to MMM), National Eye Institute (R01EY022356 to RC), National Institute of General Medical Sciences (T32GM088129 and T32GM120011 to DJD), Japan Society for the Promotion of Science Overseas Research Fellowship and Lalor Foundation (to KN). This work is partially supported by National Eye Institute grant R01EY026545 to Theodore G. Wensel (for ARM).
‡Equal contributors

Received 25 August 2019; Revised 31 December 2019; Editorial Decision 18 February 2020; Accepted 26 May 2020

Abstract

Receptor accessory protein 6 (REEP6) is a member of the REEP/Ypt-interacting protein family that we recently identified as essential for normal endoplasmic reticulum homeostasis and protein trafficking in the retina of mice and humans. Interestingly, in addition to the loss of REEP6 in our knockout (KO) mouse model recapitulating the retinal degeneration of humans with REEP6 mutations causing retinitis pigmentosa (RP), we also found that male mice are sterile. Herein, we characterize the infertility caused by loss of *Reep6*. Expression of both *Reep6* mRNA transcripts is present in the testis; however, isoform 1 becomes overexpressed during spermiogenesis. In vitro fertilization assays reveal that *Reep6* KO spermatozoa are able to bind the zona pellucida but are only able to fertilize oocytes lacking the zona pellucida. Although spermatogenesis appears normal in KO mice, cauda epididymal spermatozoa have severe motility defects and variable morphological abnormalities, including bent or absent tails. Immunofluorescent staining reveals that REEP6 expression first appears in stage IV tubules within step 15 spermatids, and REEP6 localizes to the connecting piece, midpiece, and annulus of mature spermatozoa. These data reveal an important role for REEP6 in sperm motility and morphology and is the first reported function for

a REEP protein in reproductive processes. Additionally, this work identifies a new gene potentially responsible for human infertility and has implications for patients with RP harboring mutations in *REEP6*.

Summary sentence

Receptor accessory protein 6 is essential for sperm motility, morphology, and penetration of the zona pellucida in mice.

Key words: sperm, spermatid, sperm hyperactivation, sperm motility, testis, epididymis, fertilization, male infertility, male reproductive tract..

Introduction

Infertility, the inability to conceive after 12 months of intercourse, is a condition that affects nearly 15% of couples worldwide and is attributed to a male factor in at least 50% of cases [1]. Asthenozoospermia, or reduced sperm motility, is a defect that often leads to infertility in humans due to the requirement of rigorous motility for passage through the female reproductive tract and penetration of the cumulus–oocyte complex [2, 3]. Defects in many aspects of sperm development and function can lead to asthenozoospermia, including defective axoneme formation, mitochondrial mislocalization, mislocalization of flagellar accessory structures, and many others [4]. Though new proteins governing aspects of motility are still being identified like SUN5 [5], TCTE1 [6], SSP411 [7], and CFAP69 [8], more work is needed to identify new proteins playing roles in spermiogenesis and sperm function and to elucidate their molecular functions to improve infertility diagnosis, identify targets for contraceptive development, and further basic biological understanding.

In our previous study for the transmembrane protein receptor accessory protein 6 (REEP6), we developed a knockout (KO) mouse to study the roles of REEP6 in the retina, after discovering that mutations in human *REEP6* cause retinitis pigmentosa (RP) [9, 10]. Being a member of the REEP/Yop1p family of proteins, which are well studied in somatic cells such as retinal rod cells for their roles in endoplasmic reticulum (ER) shaping and vesicle trafficking [11–17], we discovered new roles in ER and mitochondrial homeostasis and protein trafficking in rod photoreceptors for this understudied member of the REEP family [9]. An unexpected finding from our follow-up studies was that while *Reep6* KO females were fertile, *Reep6* KO males were sterile, never siring offspring throughout the entire study. Herein, we describe the characterization of *Reep6* KO male infertility and define a role for REEP6 in spermatogenesis, sperm motility, and fertilization. The work presented here is significant for the male patients identified in our previous study and to the greater public for its implications in human male fertility.

Materials and methods

Animals

All experiments involving animals were approved by the Institutional Animal Care and Use Committee (IACUC) of Baylor College of Medicine (Houston, TX) and were conducted in compliance with the guidelines and regulations for animal experimentation at this institution under protocol AN-716 in the laboratory of M.M.M. and protocol AN-4175 in the laboratory of R.C. All experiments were also in compliance with the 'Ethical Guidelines and Responsibilities' defined in the Biology of Reproduction Author Guidelines. Mice were maintained under a 12 h:12 h light:dark cycle (from 6:00 AM to 6:00 PM).

In this study, C57BL/6J male mice with heterozygous (HET) or homozygous (KO) null mutations in *Reep6* were used as generated from our previous report [9]. For all in vivo and in vitro fertilization (IVF) experiments, *Reep6* male mice were mated to wild-type (WT) female CD-1 or B6D2F1 mice from Charles River Laboratories.

Antibodies, lectins, and stains

A custom rabbit polyclonal anti-REEP6 antibody (1:1000 dilution for western blot, 1:200 for immunostaining) was kindly provided by Dr Anand Swaroop (National Eye Institute, National Institutes of Health) as described previously [13]. Mouse monoclonal anti-GAPDH-HRP was purchased from ProteinTech (product no. HRP-60004). Mouse monoclonal anti-αtubulin-AF488 was purchased (1:200 dilution; product no. 322588; ThermoFisher) to stain spermatozoa axoneme. Rabbit monoclonal anti-acetylated-α-tubulin was purchased (1:800 dilution; product no. 5335; Cell Signaling) to stain motile spermatozoa axonemes. The lectins peanut agglutinin (PNA)-FITC (1:250 dilution; product no. L7381; Sigma-Aldrich) and soybean agglutinin (SBA)-FITC were purchased (1:500 dilution; product no. FL-1011; Vector Labs). MitoTracker Red FM was purchased (400 nM dilution; product no. M7512; Invitrogen) as a mitochondrial stain. The 4′,6-diamidino-2-phenylindole (DAPI) was purchased for immunofluorescence (1 µg/mL dilution; product no. D9542; Sigma-Aldrich) as a nuclear stain. LIVE/DEAD sperm viability kit was purchased (product no. L-7011; Invitrogen) to determine sperm viability.

Western blot analysis

Testis and whole epididymis tissue were collected from adult mice (≥12 weeks) and frozen on dry ice. Frozen tissues were weighed and 100–200 mg pieces of tissue were placed in cold tissue protein extraction reagent (T-PER, ThermoFisher) and homogenized. The homogenate was centrifuged at 15 000 RPM for 15 min at 4 °C in a tabletop centrifuge. The supernatant was collected and quantified using a bicinchoninic acid protein assay kit (ThermoFisher). On a 4–12% Bis-Tris polyacrylamide gel, 30 µg of protein was loaded to each well. The proteins from the Bis-Tris gel were transferred to a PVDF membrane using the TransBlot TURBO (BioRad). Membranes were blocked with 5% skim milk in Tris-buffered saline-Tween 20 (TBST; 20 mM Tris-HCl pH 7.6, 150 mM NaCl, 0.1% Tween 20) for 1 h at room temperature (RT). Primary antibodies were diluted in blocking solution and incubated with the membranes overnight at 4 °C or 1 h at RT. Membranes were washed three times with TBST before being incubated with donkey polyclonal anti-rabbit IgG-HRP-conjugated secondary antibody (Jackson ImmunoResearch, #711-035-152) diluted 1:5000 in blocking buffer. Membranes were

washed and developed with SuperSignal West Pico PLUS chemiluminescent substrate (ThermoFisher) and imaged on a BioRad Chemi-Doc. For repeat probing of the polyvinylidene fluoride (PVDF) membrane, a 15-min incubation in mild stripping buffer (200 mM glycine pH 2.5, 1% sodium dodecyl sulfate, and 1% Tween 20) at RT was performed before washing the membrane 3× in TBS for 5 min each and repeating the blocking step for 30 min.

Reverse transcriptase-PCR

For mRNA temporal expression analysis, testes from WT B6129SF1/J hybrid mice were collected at postnatal days (PND) 3, 6, 10, 14, 21, 28, and 35 and frozen at −80 °C. These time points were selected based on the progression of testis development and the onset of the first wave of spermatogenesis [18]. Total RNA was extracted from the tissues using TRIzol reagent (Invitrogen), treated with DNaseI to remove genomic DNA, and cleaned with the RNeasy Mini Kit (Qiagen). The qScript cDNA Supermix (Quanta Biosciences) was used to generate cDNA. *Reep6* mRNA was amplified by PCR using the cDNA as a template with the following primers: (F) 5′-AGCGGAAGAGCATTGGACCTA, (R) 5′-GTGGGGTCTGACTTTACTTGG, which amplify transcript variants 1 (*Reep6.1,* 145-bp amplicon) and 2 (*Reep6.2,* 64-bp amplicon). Hypoxanthine guanine phosphoribosyl transferase (*Hprt*) was used as an expression control and amplified (400-bp amplicon) using the following primers: (F) 5′-TGGACAGGACTGAAAGACTTGCTCG, (R) 5′-GGCCTGTATCCAACACTTCGAGAGG. PCR was conducted using the GoTaq Green Master Mix (Promega) according to the manufacturer's instructions, with a final primer concentration of 500 nM and amplifying in the thermocycler for 35 cycles. An additional sample containing no cDNA input was included as a no-template control (NTC) for the PCR and was loaded onto the agarose gel as a negative control.

Histology of reproductive tissues

For periodic acid-Schiff (PAS)–hematoxylin staining, testis and whole epididymis tissues were collected from ≥8-week-old mice and fixed in Bouin's fixative (Sigma Aldrich) for 4–6 h while rotating. Tissues were then washed in 70% ethanol to remove excess fixative. Testes were cut along the transverse plane to allow for cross-sectioning. Tissues were submitted in cassettes submerged in 70% ethanol to the Baylor College of Medicine Pathology & Histology Core for processing and paraffin embedding. Embedded tissues were sectioned at 5 µm and mounted on slides. PAS–hematoxylin staining was conducted according to Ahmed and de Rooij, deparaffinized in histoclear, rehydrated from ethanol to water, stained with PAS reagent, counterstained with hematoxylin, dehydrated, cleared with Histoclear, and mounted with permount [19].

CASA and CASAnova mouse sperm motility analysis

Spermatozoa from the cauda epididymis of adult mice (≥12 weeks) were collected by dissecting the tissue and placing it in a 1.5 mL microcentrifuge tube with 1.0 mL human tubal fluid (HTF) medium (101 mM NaCl, 4.69 mM KCl, 0.2 mM $MgSO_4$, 0.37 mM KH_2PO_4, 2.04 mM $CaCl_2$, 25 mM $NaHCO_3$, 2.78 mM glucose, 0.33 mM sodium pyruvate, 21.4 mM sodium lactate, 75 µg/mL penicillin G, 50 µg/mL streptomycin sulfate, 2 µg/mL phenol red, and 9 mg/mL bovine serum albumin) pre-equilibrated in a 37 °C incubator with 5% CO_2 [20]. The tissue was minced by cutting 30 times with small scissors and placed in the incubator with the tubes ajar under 5% CO_2 for 15 min to allow spermatozoa to release. Using a wide-bore micropipette tip, spermatozoa were diluted 1:50 into 1.0 mL of fresh equilibrated media. A 20-µL sample of the dilution was placed on a chamber of 100 µm-depth counting slides (CellVision) for measuring with the CEROS II animal Computer Assisted Sperm Analysis (CASA) machine (Hamilton Thorne) and the 1:50 dilution was returned to the incubator. Sperm hyperactivity was measured from the 1:50 dilution after an additional 105 min (120 min total) of incubation. Hyperactivated spermatozoa were classified using CASAnova (https://uncnri.org/CASAnova). CASAnova is an online multiclass support vector machine (SVM) algorithm (trained with over 2000 manually classified sperm motility tracks) for classifying sperm motility patterns into vigorous (progressive, intermediate, or hyperactive) and non-vigorous motility patterns (slow or weak), as detailed in Goodson [21]. CASAnova takes five sperm kinematic measurements from CASA (average path velocity, VAP; curvilinear velocity, VCL; straight line velocity, VSL; amplitude of lateral head displacement, ALH; and beat cross frequency, BCF) into account and uses a decision tree based on equations derived from the training set to classify motility patterns. To use CASAnova, motility data for individual spermatozoa recorded by the CEROS II were exported to ASCII files, which were uploaded to the website for analysis. The CASAnova output was copied into an Excel (Microsoft) spreadsheet for data manipulation and statistical analysis.

Sperm viability analysis

Freshly released cauda epididymal sperm suspension was collected and diluted to 3×10^6 cells/mL in 1.0 mL HEPES-buffered HTF media (mHTF; 101.6 mM NaCl, 4.69 mM KCl, 0.2 mM $MgSO_4$, 0.37 mM KH_2PO_4, 2.04 $CaCl_2$, 4.0 mM $NaHCO_3$, 21.0 mM HEPES pH 7.4, 2.78 mM glucose, 0.33 mM sodium pyruvate, 21.4 mM sodium lactate, 75 µg/mL penicillin G Na salt, 50 µg/mL streptomycin sulfate, 2 µg/mL phenol red, and 5 mg/mL BSA) in a 2-mL microcentrifuge tube at 37 °C in a water bath. SYBR-14 and propidium iodide dyes were included in the LIVE/DEAD sperm viability kit to stain live spermatozoa (green) and dead spermatozoa (red) as reported [22, 23]. To each sperm suspension, SYBR-14 was diluted to a 100-nM final concentration and incubated for 10 min at 37 °C. After the incubation period, propidium iodide was diluted to a 12-µM final concentration in each sperm suspension and incubated for 10 min at 37 °C. A 20-µL sample was pipetted onto a superfrost microscope slide for each sample, cover slipped, and imaged with an epifluorescence microscope. At least 100 cells were counted per mouse and 500 cells counted per genotype. Cells were manually counted with ImageJ software (National Institutes of Health) Cell Counter plugin.

Immunofluorescent staining

For testis cryosections, tissues from adult mice were dissected and fixed in 4% paraformaldehyde (PFA) in phosphate-buffered saline (PBS; 137 mM NaCl, 2.7 mM KCl, 1.8 mM KH_2PO_4, 10 mM Na_2HPO_4 pH 7.4) + 0.1% Triton X-100 (PBTx) overnight at 4 °C. Testes were incubated in increasing sucrose/PBS buffer from 10 to 20%, allowing the testis to sink to the bottom of each tube before changing buffer. A final incubation in a 1:1 mixture of 20% sucrose:optimal cutting temperature compound (O.C.T., Tissue-Tek) for an overnight incubation at 4 °C was done before placing the tissue in a cryomold, covering with OCT, and freezing the block at −80 °C. The blocks were sectioned at 10 µm and mounted on slides. Tissue sections were blocked with PBTx + 3% BSA + 5%

normal donkey serum for 1 h at RT. Primary antibodies were diluted in blocking buffer (without Triton X-100) and incubated with sections overnight at 4 °C. Sections were washed with 3% BSA/PBS before incubating with secondary antibodies for 1 h at RT. In the final wash, DAPI was added at 1:1000 dilution in the wash buffer for 10 min. Primary antibodies used include rabbit anti-REEP6, mouse anti-αtubulin-AF488, SBA-FITC, and PNA-FITC. Secondary antibodies were donkey anti-rabbit-AF594 and donkey anti-mouse-AF488 (Life Technologies, #a21207 and a21202). Slides were imaged with a Zeiss AxioObserver Z.1 inverted fluorescence microscope. Images were processed using the Zeiss Zen Blue software version 2.6.

For spermatozoa, samples were collected from the cauda epididymis or vas deferens and allowed to swim up in HTF media for 15 min. For labeling mitochondria in spermatozoa, a freshly collected sperm suspension was prepared in 1.0 mL mHTF in a 37 °C water bath or heat block. Mitochondria were stained with a final concentration of 400 nM MitoTracker Red CMXRos (Invitrogen) according to the protocol by Sutovsky [24]. After 10-min incubation of spermatozoa with MitoTracker dye at 37 °C, cells were washed twice with PBS by centrifugation at 300 × *g* for 5 min. A 20-µL sample of spermatozoa was placed on a poly-L-lysine coated slide, and spermatozoa were allowed to bind for at least an hour before starting the immunofluorescence protocol. Otherwise, medium from the top portion of each suspension was collected and centrifuged at 300 × *g* for 5 min at RT to wash the spermatozoa in PBS. Using poly-L-lysine coated slides, 20 µL of sperm suspension was placed on slides and allowed to attach for 1 h at RT. Attached spermatozoa were fixed in 30 µL of 4% PFA/PBTx for 30 min at RT. Slides were washed in PBS, then blocked with 5% BSA/PBS for 1 h at RT. Primary antibodies were diluted in blocking buffer and incubated with spermatozoa overnight at 4 °C in a humidified chamber. Slides were washed and incubated with fluorescent secondary antibodies diluted in blocking buffer. Slides were washed with PBS for 5 min, then DAPI diluted in PBS for 10 min, then a final PBS wash for 5 min. Slides were mounted with a drop of Immu-mount aqueous medium (Thermo Fisher). Images were captured with either a Zeiss LSM 880 Confocal microscope at 63× magnification or a Zeiss AxioObserver epifluorescence microscope at 40× magnification. Fluorescence intensity of confocal microscopy images from a representative *Reep6* HET and *Reep6* KO mouse epididymal spermatozoa was quantified using ImageJ [25]. For both HET and KO mice, five field images of sperm were captured, containing a total of at least 50 spermatozoa, and fluorescence intensity for each field was determined by ImageJ. The raw fluorescence intensity of each field was normalized by dividing by the number of spermatozoa in the corresponding field. The resulting intensity/sperm values for the HET and KO mouse were analyzed for statistical differences by a Student's *t*-test and represented as the mean intensity/spermatozoa ± standard error of the mean (SEM).

In vivo and in vitro fertilization analysis

For in vivo fertilization analysis, 3-week-old B6129SF1/J hybrid female mice were superovulated by I.P. injection with 5 IU pregnant mare serum gonadotropin (PMSG) (0.1 mL/mouse) in the evening and a follow-up injection of 5 IU hCG after 48 h. After injection of hCG, two superovulated females were mated in a trio to a single *Reep6* HET or KO mouse overnight. The next morning, females were checked for copulation plugs. Females with copulation plugs were euthanized using isofluorane followed by cervical dislocation, and zygotes or unfertilized oocytes were subsequently collected from the oviducts by dissecting and flushing them with HTF media. Collected zygotes/oocytes were inspected for the presence of two pronuclei and extrusion of the polar body. Zygotes/oocytes were cultured overnight in a 37 °C incubator under 5% CO_2 and observed for progression to the two-cell stage.

The IVF experiments were performed as described previously [26].

Induced acrosome reaction

Spermatozoa from the cauda epididymis of adult mice were released by mincing the tissue 30 times in 1.0 mL equilibrated HTF media and incubating for 15 min at 37 °C under 5% CO_2. The sperm suspension was then diluted to 1 × 10^6 cells/mL in 1.0 mL fresh HTF and incubated for 120 min at 37 °C under 5% CO_2. A 5-mM stock of the calcium ionophore A23187 prepared in dimethyl sulfoxide (DMSO) or a DMSO control was diluted 1:500 into the sperm suspension for a final concentration of 10 µM A23187, as we previously reported [27]. Sperm samples were incubated under CO_2 for 1 h to allow the acrosome reaction to complete. Finally, the treated sperm samples were washed twice in PBS, mounted on slides, stained with PNA to assess the acrosomal status and counterstained with DAPI. Slides were imaged with a Zeiss AxioObserver epifluorescence microscope at 40× magnification. At least 200 spermatozoa were counted per mouse.

Sperm population counting

Spermatozoa from the cauda epididymis of adult mice were released by making a single cut in the cauda with fine scissors and dragging the sperm fluid into 1.0 mL equilibrated HTF media. The sperm suspension was incubated for 15 min at 37 °C under 5% CO_2 to allow spermatozoa to disperse. Spermatozoa were diluted 1:50 into fresh 1.0 mL equilibrated HTF media. A 20-µL sample was placed on a microscope slide, cover slipped, and incubated in a humidified chamber until spermatozoa were no longer motile. Spermatozoa were imaged using phase contrast microscopy at 20× magnification. For each analysis, at least 80 spermatozoa were counted per mouse and at least 400 spermatozoa combined were counted per genotype using ImageJ (NIH) with the cell counter plugin.

Scanning electron microscopy and transmission electron microscopy

For scanning electron microscopy (SEM) of spermatozoa, a single cut was made in cauda epididymis tissue and using fine tweezers, fluid released from the epididymis was placed in a 2-mL microcentrifuge tube with 1.0 mL equilibrated TYH media + 4 mg/mL BSA (119.37 mM NaCl, 4.78 mM KCl, 1.19 mM $MgSO_4$, 1.19 mM KH_2PO_4, 1.71 mM $CaCl_2$, 25.07 mM $NaHCO_3$, 5.56 mM glucose, 1 mM sodium pyruvate, 75 µg/mL penicillin G, 50 µg/mL streptomycin sulfate, and 2 µg/mL phenol red) [28]. Spermatozoa were incubated for 15 min at 37 °C under 5% CO_2 to allow spermatozoa to disperse, then centrifuged at 300 × *g* for 5 min at RT and resuspended in Dulbecco PBS (DPBS) to wash. Spermatozoa were centrifuged again and resuspended in 2.5% glutaraldehyde in DPBS for 30 min at RT to fix. Spermatozoa were washed in increasing concentrations of ethanol from 20 to 100% to dehydrate, incubating for 10 min in each. Spermatozoa were centrifuged at 1500 × *g* for 5 min at RT and resuspended in 50% t-butanol/50% ethanol for 15 min at RT. A 20-µL sample of sperm suspension was dried on a specimen pin mount. The samples were sputter-coated with iridium before imaging.

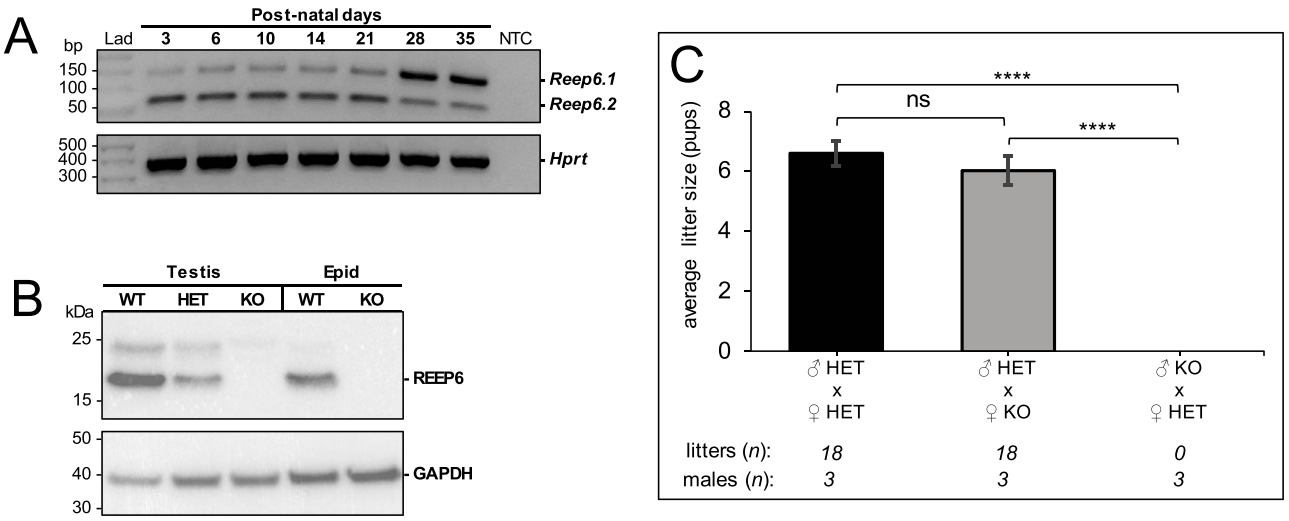

Figure 1. Analysis of *Reep6* expression profile and fertility assessment of KO males. (A) RT-PCR of mouse testis mRNA from PND 3 to 35, amplifying the two transcript variants of *Reep6* and using *Hprt* as an expression control. Lane 1, labeled "Lad," contains the DNA ladder. A NTC was included in the final lane. (B) Western blot of 30 µg per lane testis and whole epididymis extracts from adult *Reep6* WT, HET, and KO mice using GAPDH as an expression control. Both REEP6 isoforms, REEP6.1 (22.2 kDa) and REEP6.2 (19.4 kDa), were absent in *Reep6* KO testis and epididymis. (C) Mating analysis data from trio breedings of *Reep6* HET and KO mice, counting 6 L per male from three males in each breeding group. Mean litter size was calculated as the number of live pups born per number of birthing events. Error bars represent SEM. Analyzed by one-way ANOVA with Tukey–Kramer post-hoc test. Not significant (ns), $P < 0.05$ (*), $P < 0.01$ (**), $P < 0.001$ (***), and $P < 0.0001$ (****).

For transmission electron microscopy (TEM) of testes, mice were injected via I.P. with 0.01 mL/g ketamine–xylazine to anesthetize. Mice were then fixed with 2.5% glutaraldehyde in DPBS by transcardial perfusion with a peristaltic pump. Testes and cauda epididymis were dissected and placed in fixative overnight at 4 °C. Tissues were washed with PBS and incubated with 1% osmium tetroxide in cacodylate buffer for 2 h at RT. After dehydration with 30, 50, 70, 90% ethanol, 90% acetone, and 100% acetone, tissues were incubated in 50% resin/50% acetone for 2 h, followed by 66% resin/33% acetone overnight, and finally in 100% resin for 3 h. Samples were then embedded in 100% resin and embedded molds were incubated at 60 °C for 48 h. Ultrathin 100-nm tissue sections were cut with a diamond knife and mounted on a copper grid. Sections were stained with uranyl acetate and lead citrate.

Statistical analysis

For all interval data, statistical significance between two groups was determined using a two-tailed Student's *t*-test assuming unequal variances with an α level of 0.05. Significance between more than two groups of interval data was determined by one-way ANOVA with a post-hoc Tukey–Kramer HSD test. For nominal data, statistical significance was determined either by a Chi-square test of independence followed a Fisher's exact test or by calculating the adjusted standard residuals for post-hoc testing. *P* values less than 0.05 were considered significant. All statistical analyses were performed using Microsoft Office Excel with the Analysis ToolPak and RealStats plug-ins (www.real-statistics.com/free-download/).

Results

Reep6 KO male mice are sterile

Since *Reep6* has two major isoforms that differ in the inclusion (*Reep6.1*) or exclusion (*Reep6.2*) of exon 5, we wanted to investigate the temporal expression of *Reep6* transcript variants during testis development [12]. Reverse transcriptase (RT)-PCR analysis of WT mouse testis tissue from PND 3 to 35 revealed that both isoforms are expressed throughout testis development; however, expression of *Reep6.1* (the full-length transcript) spikes at PND 28 (Figure 1A). This corresponds with the appearance of the first round spermatids at PND 18 [18]. In our previous report [9], we demonstrated the loss of REEP6 from the retina in our KO mouse via immunofluorescence. To confirm loss of REEP6 from the male reproductive tract in our KO model, we performed western blot analysis of testis and epididymis tissue from adult KO and control males. The approximately 20-kDa REEP6 protein is reduced in the testis of HET males and is absent in the testis and epididymis of KO males (Figure 1B). We also noted that *Reep6* KO female mice were fertile, based on progeny produced from KO females bred to HET males. To examine the fertility of KO males, 8-week-old *Reep6* KO males were mated to *Reep6* HET females for several months. *Reep6* KO males were found to be completely infertile, siring no litters within the breeding period (Figure 1C). Mating behavior for *Reep6* KO males was normal; males were observed to successfully produce copulation plugs similar to HET controls. In contrast to KO males, the mean litter size of *Reep6* KO females was 6.0 ± 0.5 and was comparable with the 6.6 ± 0.4 mean litter size of heterozygous controls, confirming that *Reep6* KO females are fertile. These data indicate that *Reep6* is essential for male fertility in mice.

Reep6 KO spermatozoa are unable to penetrate the zona pellucida

To further assess the cause of *Reep6* KO male infertility, *Reep6* HET and *Reep6* KO males were mated to superovulated WT B6129SF1/J females, and after mating, the oviducts were collected and flushed. The collected zygotes or unfertilized oocytes were cultured overnight to allow progression to the two-cell stage to determine if fertilization had occurred. *Reep6* HET males successfully fertilized 90.7 ± 2.7% of oocytes that progressed to the two-cell stage, while *Reep6* KO

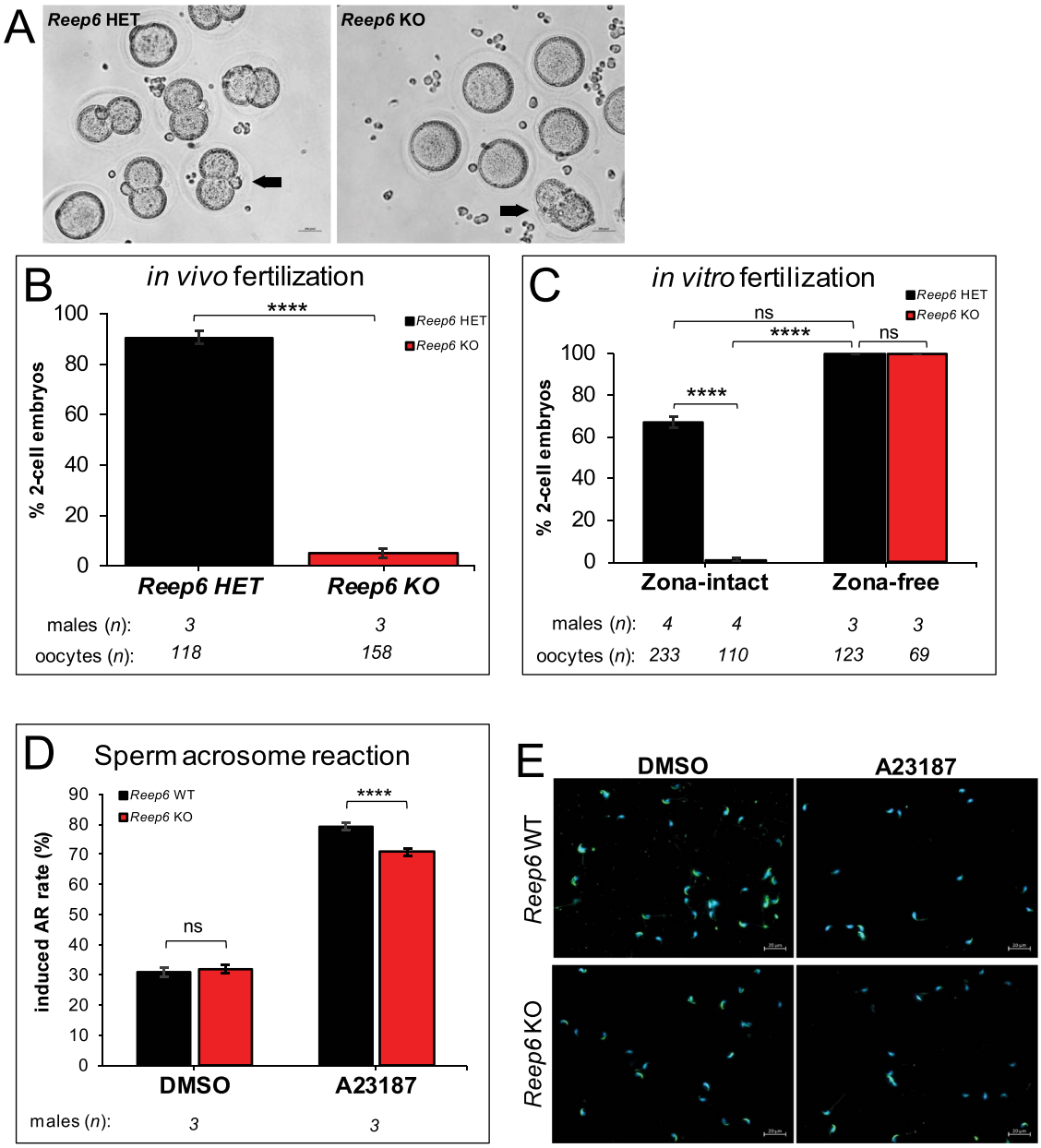

Figure 2. In vivo and IVF analysis of *Reep6* KO spermatozoa. (A) Light microscopy images of oocytes/zygotes 48 h post-coitus from natural mating of *Reep6* HET or KO males to superovulated WT females. Arrows show fertilized oocytes that have progressed to two-cell stage embryos. (B) Quantification of two-cell embryos from in vivo fertilization by trio mating *Reep6* HET and KO males to two WT females each. Three males of each genotype were used in each mating group. (C) Quantification of two-cell embryos from IVF using spermatozoa from *Reep6* HET and KO males and oocytes from superovulated WT females. Oocytes with intact zona pellucida or zona-free oocytes were prepared for the IVF experiment. Percent two-cell embryos were calculated as the number of fertilized oocytes divided by the number of total oocytes collected. (D) Quantified comparison of sperm acrosome exocytosis between WT and *Reep6* KO spermatozoa by induction with 10 μM A23187 or DMSO as a negative control. Data represent three independent experiments using $n = 3$ males for each genotype. At least 1200 total spermatozoa were counted for each treatment group. (E) Representative images of spermatozoa from each of the acrosome reaction assay treatment groups. PNA–FITC (green) was used to stain the acrosome, while DAPI (blue) was used to stain sperm nuclei. Images were taken at 40× magnification. Error bars represent standard error (SE) for independent sample proportions. Analyzed by Chi-square test of independence with adjusted standard residual or Fisher's exact test post-hoc testing. Not significant (ns), $P < 0.05$ (*), $P < 0.01$ (**), $P < 0.001$ (***), and $P < 0.0001$ (****).

males fertilized only 5.1 ± 1.7% of oocytes that progressed to the two-cell stage (Figure 2A and B). Under the microscope, it was evident that *Reep6* spermatozoa were able to bind the zona pellucida, but perhaps were unable to penetrate. To test whether penetration of the zona pellucida was the source of fertilization failure in *Reep6* KO males, spermatozoa from *Reep6* HET and *Reep6* KO males were used in zona-free versus zona-intact IVF experiments. Both *Reep6* HET and *Reep6* KO spermatozoa were able to fertilize 100% of zona-free oocytes; however, *Reep6* KO spermatozoa were unable to fertilize zona-intact oocytes 0.9 ± 0.9% (Figure 2C). To confirm that Reep6 KO spermatozoa were able to bind the zona pellucida, the acrosome reaction was induced using the calcium ionophore A23187, as most spermatozoa undergo the acrosome reaction before binding the zona pellucida [29]. After treating WT and KO

spermatozoa with either 10 μM A23187 or DMSO control, KO spermatozoa were able to execute acrosomal exocytosis (70.9 ± 1.2%), although slightly decreased compared with WT spermatozoa (79.3 ± 1.1%) (Figure 2D and E). These data highlight that REEP6 is needed for spermatozoa to penetrate the zona pellucida, although it is not essential for the ability of sperm to bind this structure.

Loss of *Reep6* causes epididymal sperm abnormalities

To better understand why *Reep6* KO spermatozoa are unable to penetrate the zona pellucida, we first examined the testes, in which there were no differences between the sizes of *Reep6* HET and *Reep6* KO mice (Figure 3A and B). There was also no significant difference in the average body weight between the two groups of mice (supplementary Figure S1A and B). Upon examining the testis histology with PAS–hematoxylin staining, there were no clear aberrations in spermatogenesis (Figure 3C). Although all generations of spermatids seemed to be present, there were appearances of atypical residual bodies remaining toward or within the lumen in some stage IX tubules of *Reep6* KO mice (supplementary Figure S2). Histological sections of the cauda epididymis revealed that the lumen of *Reep6* HET mice appeared normal and was filled with spermatozoa (Figure 3D, left), while the lumen of *Reep6* KO mice contained large, round cell masses, which are likely the atypical residual bodies from the testis (Figure 3D, right). In addition, cauda epididymal sperm counts were 28% reduced in *Reep6* KO (30.2 ± 4.3 × 10^6 cells) compared with *Reep6* HET controls (42.1 ± 3.7 × 10^6 cells), suggesting lower sperm production or degradation of defective spermatozoa (Figure 3E) [30]. *Reep6* KO spermatozoa also exhibited various morphological abnormalities when compared with WT spermatozoa, including significantly reduced normal sperm morphology (7.9 ± 1.2% vs. 31.5 ± 2.2%) mostly because of a significant increase in tails bent at the annulus (41.6 ± 2.1% vs. 20.3 ± 1.9%) or absent tails (13.3 ± 1.5% vs. 3.6 ± 0.9%) (Figure 3F and G). The annulus is a ring-like diffusion barrier between the midpiece of the sperm tail and the principal piece [4]. These data suggest that REEP6 has a role in late spermiogenesis that, when perturbed, disrupts the annulus, disturbs proper head-tail coupling, and leads to abnormal epididymis histology.

Reep6 KO spermatozoa demonstrate severe loss of motility

To assess the motility of *Reep6* HET and *Reep6* KO spermatozoa, CASA was conducted to assess general sperm motility and kinematics, while CASAnova was subsequently performed to classify the types of motility on sperm extracted from the cauda epididymis of adult mice. All nominal variables (percent of spermatozoa counted per category) were analyzed using the Chi-square test of independence with a Fisher's exact test for post-hoc analysis. All integer variables (measured sperm kinematics) were analyzed with a Student's *t*-test assuming unequal variances. The percent of total motile *Reep6* KO spermatozoa was significantly reduced (7.64 ± 0.3%) compared with *Reep6* HET spermatozoa (43.3 ± 0.8% of total spermatozoa) (Figure 4A). Representative videos from CASA analysis illustrate the stark difference in motility between HET (supplementary Figure S3 and supplementary Movie 1) and KO spermatozoa (supplementary Figure S3 and supplementary Movie 2), as there are significantly fewer motile sperm tracks (marked in green) in KO sperm samples. *Reep6* KO spermatozoa also exhibited significantly reduced progressive motility (3.91 ± 0.2%) compared with controls (29.2 ± 0.7%) (Figure 4B). After incubating spermatozoa for 120 min in HTF to allow capacitation [31–33], the spermatozoa were reanalyzed for hyperactivation and other motility classifications using the CASAnova SVM. Although slightly reduced, there was no significant difference in the level of hyperactivation among motile spermatozoa between *Reep6* HET (5.15 ± 0.8%) and KO (2.20 ± 0.5%) mice after 120 min (Figure 4C). This observation demonstrates that although there are far fewer motile spermatozoa in the *Reep6* KO epididymis, the spermatozoa that are motile are able to hyperactivate. Hyperactivation is an essential component of sperm capacitation (the acquisition of fertilizing capability) [31, 32, 34]. CASAnova also classifies sperm motility into intermediate, slow, and weak motility profiles (supplementary Figure S1C). *Reep6* KO spermatozoa exhibited significantly higher percentages of slow (79.1 ± 1.4% vs. 30.7 ± 1.6%) and weak (3.3 ± 0.6% vs. 0%) motility profiles compared with HET control spermatozoa after 120 min (supplementary Table S1). The CASAnova data were in agreement with the sperm kinematic data from CASA, as all three measurements (average path velocity, VAP; curvilinear velocity, VCL; and straight-line velocity, VSL) [35] were significantly reduced in *Reep6* KO spermatozoa (Figure 4D–F). Finally, to ensure that the poor motility of the *Reep6* KO spermatozoa was due to a motility-specific defect and not caused by cell death, spermatozoa from WT and KO mice were co-stained with SYBR-14 to label living (membrane-intact) cells and propidium iodide to label dead (membrane-disrupted) cells [22]. Although there was a significant reduction in KO sperm viability (31.0 ± 1.0%) compared with WT controls (35.7 ± 1.1%) determined by a Chi-square test of independence and Fisher's exact post-hoc test, this slight reduction does not account for the severe reduction in motility (Figure 4G and H). These data suggest that REEP6 has a critical role in sperm motility and highlight that loss of *Reep6* leads to a severe motility defect.

REEP6 localizes to the connecting piece and midpiece of spermatozoa

To determine the subcellular localization of REEP6, an anti-REEP6 antibody was used in immunofluorescence experiments within the testis and spermatozoa of *Reep6* HET and *Reep6* KO specimens. Within the seminiferous tubules, REEP6 localized to midpiece of elongating spermatids (Figure 5A). The earliest appearance of REEP6 staining is in the midpiece of step 15 spermatids in stage IV seminiferous tubules [36]. The signal is strongest in stages VII–VIII seminiferous tubules, as step 16 spermatids prepare for spermiation. Within spermatozoa collected from the cauda epididymis, REEP6 demonstrates more pronounced localization at two focal points: the connecting piece and the annulus as the base of the midpiece (Figure 5B). REEP6 staining is also prominent along the entire midpiece. As expected, no REEP6 signal is observed in *Reep6* KO testis and spermatozoa. To investigate the mitochondria integrity of *Reep6* KO sperm, spermatozoa were labeled with MitoTracker Red. In addition, the status of acetylated α-tubulin was investigated, as its expression has been reported to be reduced in cases of poor sperm motility [37]. Structural integrity of the midpiece and the mitochondria were not noticeably compromised by the loss of REEP6 (Figure 5C). There were also no significant differences in the fluorescence intensity of MitoTracker or acetylated α-tubulin staining between HET and KO spermatozoa (Figure 5D). These data suggest that the motility deficit and sperm tail defects in *Reep6*

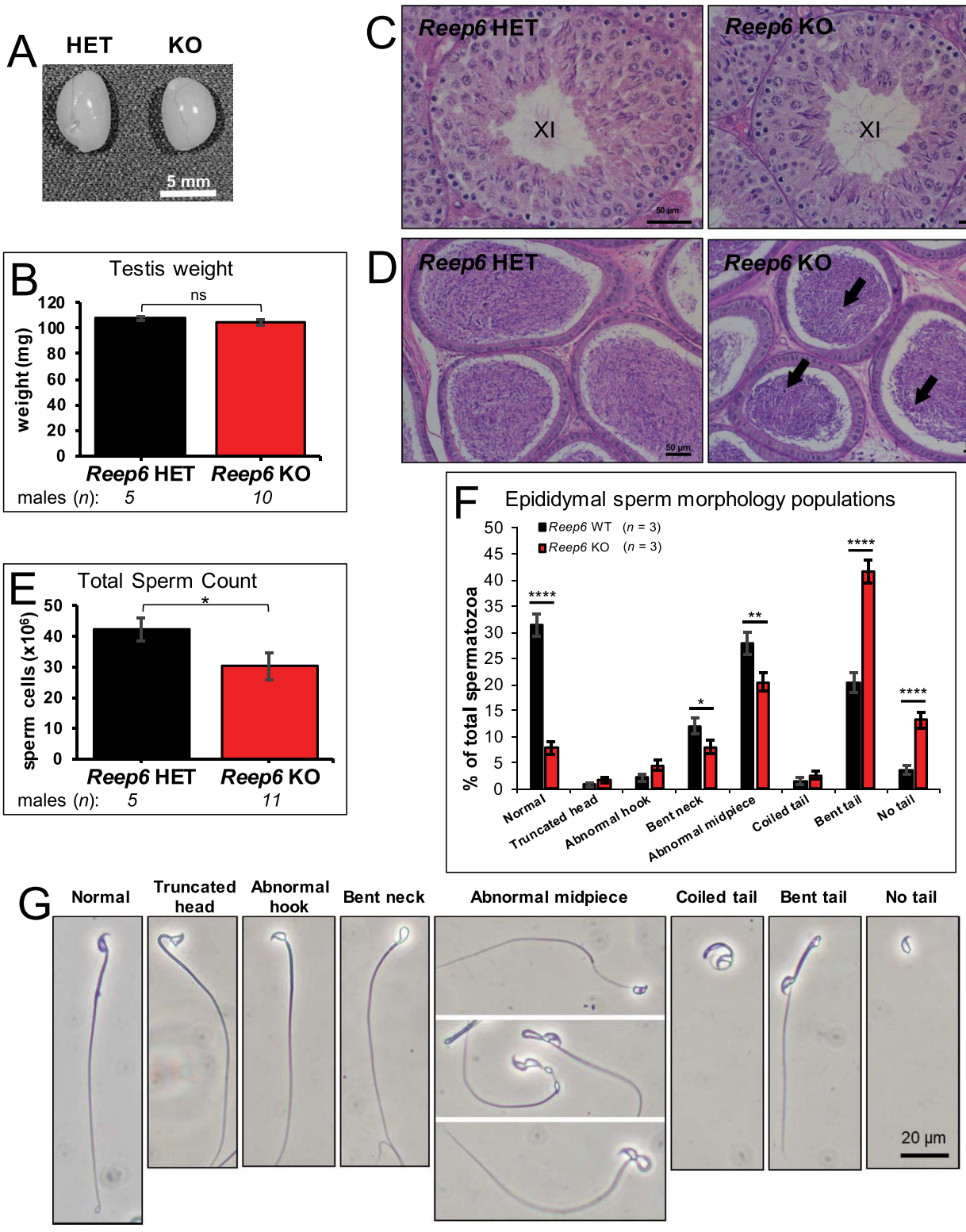

Figure 3. Gross and histological characterization of *Reep6* KO consequences in the testis, epididymis, and spermatozoa. (A) Representative whole testis images and (B) gross testis weights from *Reep6* HET and KO mice. (C) PAS–hematoxylin staining of testis cross-sections from HET and KO mice showing individual seminiferous tubules in stage XI. Images were taken at 40× magnification. (D) PAS–hematoxylin staining of the cauda epididymis from HET and KO mice. Arrows indicate abnormal round cells in the epididymal lumen. Images were taken at 20× magnification. (E) Quantification of cauda epididymal spermatozoa extracted from HET and KO mice. Total sperm count was calculated as the number of spermatozoa counted from a 1:50 dilution in 1 mL of HTF media, represented as an average for each group. Error bars represent SEM. Analyzed by a Student's *t*-test. (F) Quantification of sperm morphology populations in WT and KO mouse cauda epididymis. Error bars represent SE of independent sample proportions. Analyzed by a Chi-square test of independence with adjusted standard residual post-hoc testing. (G) Representative phase contrast microscopy images of the various sperm populations in WT and KO mice taken at 20× magnification. Not significant (ns), $P < 0.05$ (*), $P < 0.01$ (**), $P < 0.001$ (***), and $P < 0.0001$ (****).

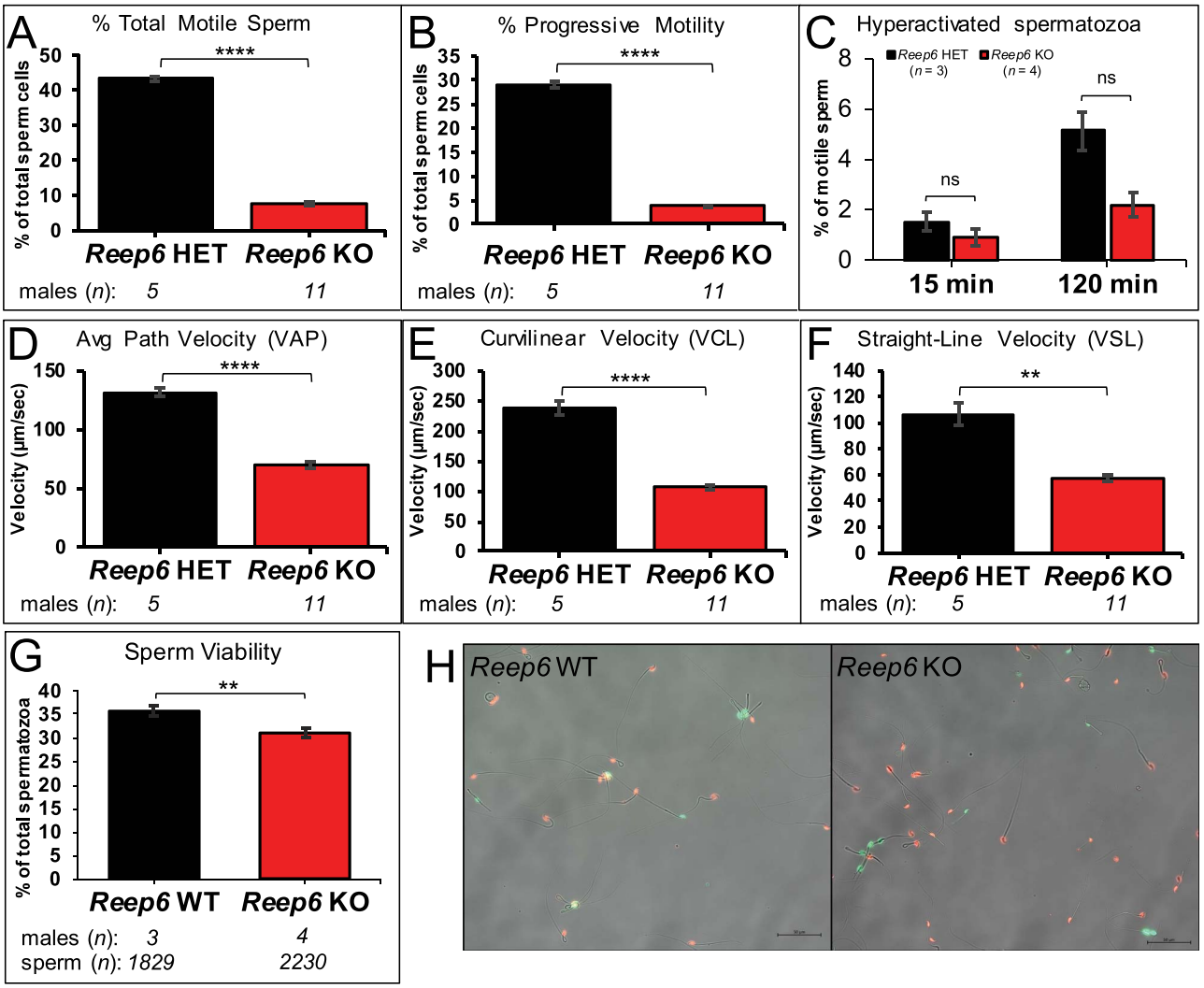

Figure 4. Motility analysis by CASA for *Reep6* HET and KO spermatozoa. (A–C) Classification of sperm motility by CASA and CASAnova. Error bars represent SE. Data analyzed by a Chi-square test of independence with a post-hoc Fisher's exact test. (A) Assessment of total sperm motility was calculated by counting sperm movement irrespective of the pattern. (B) Assessment of progressive motility derived from counting only spermatozoa moving in progressive forward motion. (C) Comparison of hyperactivation between *Reep6* HET ($n = 3$) and KO ($n = 4$) spermatozoa by CASAnova classification was assessed at 15 min and again after incubating for 120 min in HTF media. The percent hyperactivated sperm increases after capacitation in normal motile spermatozoa. (D–F) Sperm kinematic analysis by CASA for *Reep6* HET and KO spermatozoa, measuring mean sperm directional velocities (D) VAP, (E) VCL, and (F) VSL. Error bars represent SEM. Analyzed by a two-tailed Student's *t*-test assuming unequal variance. Several fields of sperm were captured so that at least 400 spermatozoa were analyzed per mouse. (G) Quantification of a sperm viability assay comparing WT and KO spermatozoa. Error bars represent SE. Analyzed by Chi-square test of independence with a post-hoc Fisher's exact test. Not significant (ns), $P < 0.05$ (*), $P < 0.01$ (**), $P < 0.001$ (***), and $P < 0.0001$ (****). (H) Representative images of the sperm viability assay. Live spermatozoa stained with SYBR-14 (green) and dead spermatozoa stained with propidium iodide (red) are presented at 20× magnification.

KO spermatozoa are not directly due to mitochondrial or sperm axoneme defects.

To assess the *Reep6* KO sperm defects in greater detail, SEM was used to image sperm extracted from the cauda epididymis. Compared with WT mouse spermatozoa (Figure 6A–C), *Reep6* KO spermatozoa (Figure 6D–F) exhibited abnormal head morphology including truncated sperm head, abnormally wide sperm head, and sperm with a sharp bend in the tail at the annulus—a common feature of a defective annulus [4]. These observations were in agreement with the sperm populations quantified from phase contrast microscopy (Figure 3F and G). To look at the ultrastructural differences in WT and *Reep6* KO spermatids throughout spermatogenesis, TEM images from the testes were analyzed. Elongated spermatids (steps 15–16) in the WT testis showed proper head and nuclear shaping, while some elongated spermatids in *Reep6* KO testes, presented with abnormal head morphology (Figure 6G). This observation, in agreement with the sperm populations identified in Figures 3F and 6D, is indicative of manchette abnormalities in the *Reep6* KO, as abnormalities in the manchette and intramanchette transport (IMT) can lead to sperm head shape defects [4, 38–40]. Despite this defect, however, other spermatids in the KO testis appeared normal and the axoneme microtubule 9 + 2 structure was unaffected in both WT and *Reep6* KO testes (supplementary Figure S4).

Discussion

REEP6 is a member of a group of REEP proteins, belonging to the Ypt-interacting protein family, that were discovered for their ability to enhance the expression of G protein-coupled receptors (GPCRs)

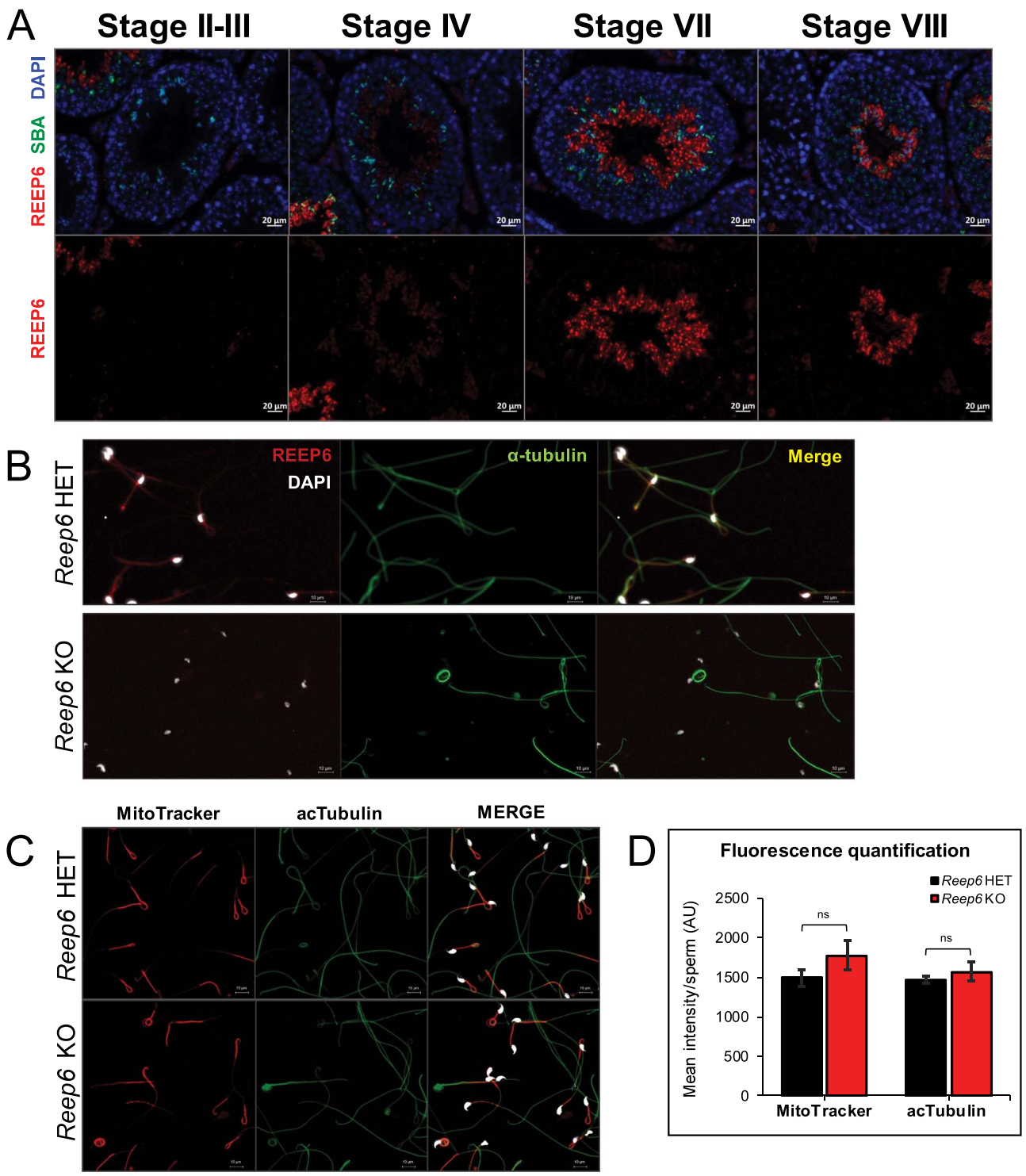

Figure 5. REEP6 subcellular localization in testis and spermatozoa. (A) Immunofluorescent staining of adult WT mouse testis cryosections showing different stages of the cycle of seminiferous epithelium. Anti-REEP6 (red) is indirectly stained t, SBA-FITC (green) is used to mark the acrosome of spermatids, and DAPI (blue) marks the nucleus. (B) Immunofluorescent staining of cauda epididymal spermatozoa from *Reep6* HET and KO mice. Anti-REEP6 (red) is used to label REEP6, anti-α-tubulin (green) is used to mark the flagella, and DAPI (white) marks the nucleus. (C) Immunofluorescent staining to evaluate mitochondria and axoneme structure in *Reep6* HET and KO cauda epididymal spermatozoa. MitoTracker (red) is used to stain mitochondria in the midpiece, anti-acetylated α-tubulin (acTubulin, green) is used to mark the axoneme, and DAPI (white) marks the nucleus. (D) Fluorescence quantification of MitoTracker and acTubulin staining in *Reep6* HET and KO cauda epididymal spermatozoa using ImageJ. Quantification was conducted from five raw images each from a representative *Reep6* HET and *Reep6* KO mouse, which included at least 50 spermatozoa for each genotype. The raw fluorescence intensity of each image was divided by the number of spermatozoa in the corresponding image, giving an intensity per sperm value. The fluorescence intensity per sperm values for the *Reep6* HET and KO was analyzed using a Student's *t*-test. Not significant (ns). Arbitrary units (AU). Error bars represent SEM.

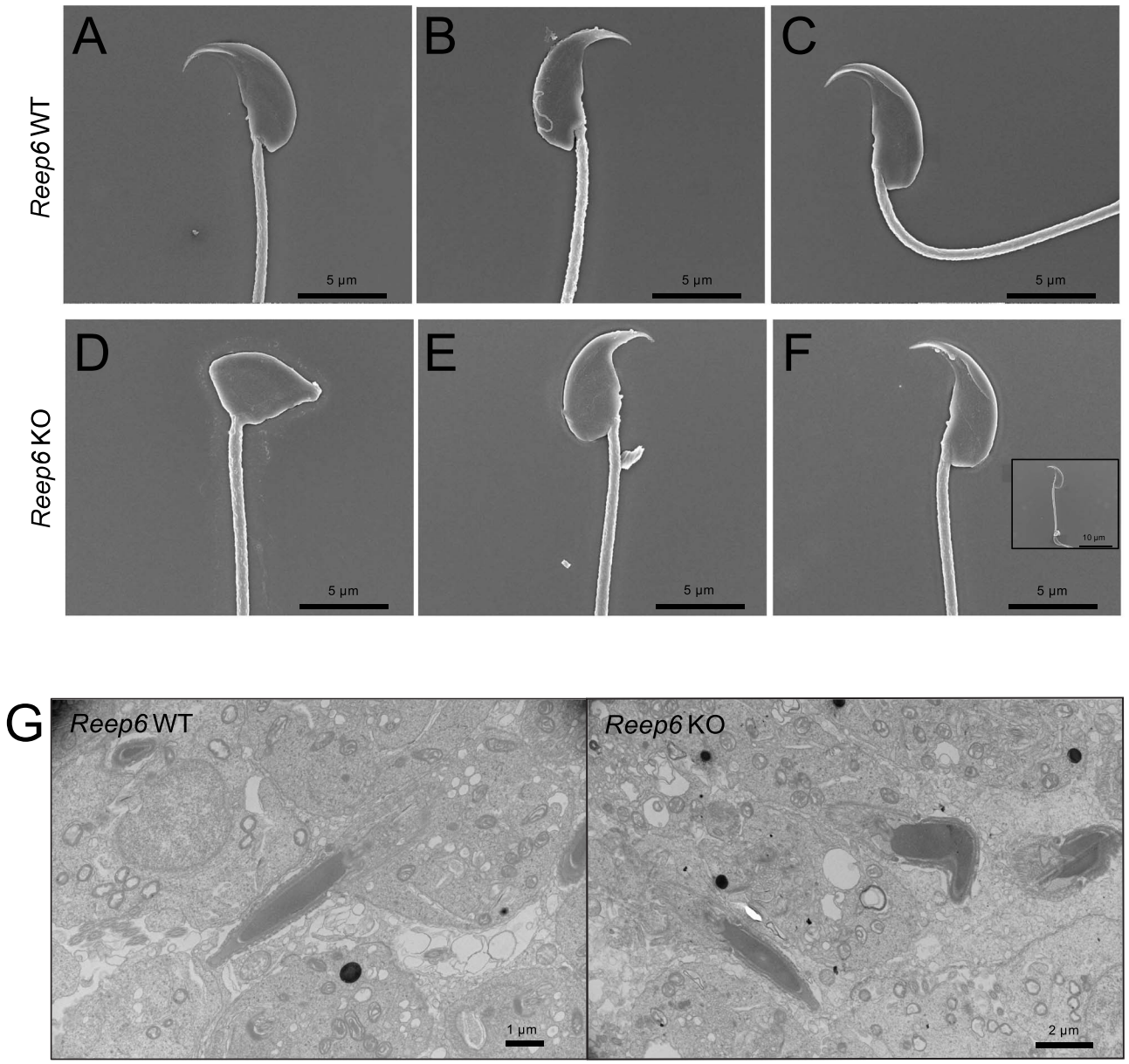

Figure 6. Ultrastructural characterization of *Reep6* KO testis and spermatozoa. (A–C) SEM images of cauda epididymal spermatozoa from WT mice displaying normal morphology. (D–F) SEM images of *Reep6* KO (bottom) spermatozoa showing (D and E) abnormal sperm head morphology and (F) normal head morphology, but abnormal bending of the tail at the annulus (inset, 9114× magnification). Images were taken at 15 000× magnification. (G) TEM of testis sections from WT (left, 4000× magnification) and *Reep6* KO (right, 3000× magnification) mice showing sections through steps 15–16 spermatids.

on the surface of cells in in-vitro culture systems [11]. In somatic cells, REEP proteins localize primarily to the ER and have various roles in modulating ER structure, regulating ER–Golgi transport, and localization of cargo proteins. The importance of REEP6 was highlighted in the development of rod photoreceptors, as its elevated expression was first discovered in the mouse retina, a retina-specific isoform was discovered in mice, and we previously reported that human mutations in *REEP6* cause RP, the most common inherited retinal disease [10, 12, 17]. In our recent report, we evaluated a CRISPR/Cas9-generated *Reep6* KO mouse model and showed that loss of REEP6 led to retinal degeneration caused by ER dysregulation, abnormal mitochondria proliferation, mislocalization of retinal guanylate cyclases, and induction of ER stress [9]. Throughout these studies, fertility did not appear to be affected when initially analyzed from *Reep6* KO female matings; however, after noticing *Reep6* KO males sired no pups over the entire study length, despite evidence of copulation plugs, we initiated an investigation of male fertility.

It was previously established that *Reep6* has two major transcripts, with the larger one, *Reep6.1*, exhibiting retina-specific expression [12]. After examining the temporal expression of both *Reep6* isoforms during testis development, we found that the *Reep6.1* isoform is predominant. However, since the retina of the eye is part of the central nervous system and considerable expression similarities between the brain and testis have been reported in humans and mice, this finding is not alarming [12, 41]. Instead, it is suggestive that REEP6 plays a similar role in the testis as it does in the retina. Using our established *Reep6* KO line, we demonstrate herein that *Reep6* KO males are sterile and sire no offspring from natural mating. Upon further investigation, we learned that *Reep6* KO spermatozoa are only able to fertilize

zona-free oocytes, revealing that REEP6 is required for penetration of the zona pellucida. *Reep6* KO spermatozoa were able to bind the zona pellucida, indicating that REEP6 is not necessary for zona pellucida binding. CASA and CASAnova analysis of *Reep6* KO spermatozoa was critical in revealing that loss of REEP6 leads to a drastic loss of motility. Demonstrating that *Reep6* KO spermatozoa can undergo acrosome reactions (Figure 2D and E) provided evidence that the spermatozoa could bind the zona pellucida; however, the severe motility defect provides an answer for why *Reep6* KO spermatozoa are unable to penetrate the zona pellucida. This also suggests that it is more difficult for KO males to impregnate females because the spermatozoa are not motile enough to traverse the female reproductive tract. Although there are far fewer motile spermatozoa present in the *Reep6* KO epididymis, the spermatozoa that are motile are capable of hyperactivation (Figure 4C) and are likely the explanation for the few fertilized eggs in the in vivo fertilization experiment (Figure 2B).

Spermatogenesis in *Reep6* KO testes was evaluated using PAS–hematoxylin staining [19, 42] and appeared normal, as all steps of spermatid development could be identified (Figure 3C). However, in many tubules in stage IX of the seminiferous epithelium, large atypical residual bodies were left in the lumen after spermiation (supplementary Figure S2). This defect is indicative of abnormal spermatid cytoplasm removal due to defective disengagement from the ectoplasmic specialization (ES) junction to the sertoli cell [43, 44]. This abnormal spermatid cytoplasm is likely the explanation for the round masses in the *Reep6* KO epididymal lumen (Figure 3D). MAKORIN-2 is another protein recently described with a similar defect [45]. Another unexpected finding was that the loss of REEP6 also leads to abnormal truncated and abnormal apical hook head shapes (Figure 3G). Although the acrosome remains an intact structure in *Reep6* KO sperm, several of the sperm heads are misshapen (Figure 2E). A review by O'Donnell [43] highlighted that abnormalities in the manchette during spermiogenesis can cause sperm head shape defects; however, we have not found evidence of manchette defects here. The two most significant abnormalities in *Reep6* KO spermatozoa were tails bent at the annulus and detached sperm heads. The annulus is a ring-like structure, made up of a complex of septin proteins, which migrates toward the fibrous sheath border during late spermiogenesis as mitochondria assemble into the midpiece behind it [46, 47]. As reviewed by Lehti and Sironen [4], loss of proteins involved in annulus formation often leads to bent tails and defective motility, suggesting a potential role for REEP6 in this process. Similarly, it was recently reported that sad1 and unc84 domain containing 5 (SUN5) is a protein that localizes to the sperm head–tail coupling apparatus (HTCA) in the connecting piece and mediated sperm head attachment [5]. *Sun5* KO led to detached sperm heads, like that seen in *Reep6* KO spermatozoa. Immunofluorescence staining in the testis and spermatozoa revealed that REEP6 expression appears in stage IV seminiferous tubules within step 15 spermatids and is present until the release of step 16 spermatids in stage VIII. In mature spermatozoa, REEP6 localizes to the connecting piece, midpiece, and annulus. These final two steps of spermatid development see the disappearance of the manchette by an unknown mechanism, the formation of the annulus, and mitochondria assembly in the midpiece [4, 40]. Given the late appearance of REEP6 in spermiogenesis and its localization pattern, it may have a role in these processes. Also, due to the appearance of detached sperm heads in *Reep6* KO epididymal sperm and REEP6's localization to the connecting piece, it may play a role in the HTCA, similar to SUN5. A reported mouse KO model for kinase suppressor of Ras 2 (KSR2) found that loss of KSR2 leads to nuclear shape defects and sperm with detached heads, similar to our findings with REEP6 [4, 48]. Future proteomic studies will be beneficial in identifying the true molecular roles and interactions of REEP6 in these various processes during spermiogenesis and sperm tail function.

TEM revealed a normal 9 + 2 axoneme microtubule organization in absence of REEP6 (supplementary Figure S4). This observation suggests that the cause of motility defects in *Reep6* KO spermatozoa is not due to structural defects of the tail and, instead, could be due to the mislocalization of accessory proteins for tail function (motor proteins, ion channels, etc.). We recently reported on the sperm flagella protein, T-complex associated testis expressed 1 (*Tcte1*) [6], in which gene KO in mice caused male sterility due to motility defects. In that study, we found that TCTE1 was part of the nexin–dynein regulatory complex (N-DRC), a critical motility component that provides resistance to microtubule sliding and assists doublet alignment in the flagellum [49]. Akin to the *Reep6* KO, *Tcte1* KO did not affect the axoneme structure, but instead, is required for metabolism and ATP generation. Due to the severe motility defects in *Reep6* KO mice and REEP6 midpiece localization, it would be interesting to investigate whether REEP6 also has a role related to N-DRC function.

These studies have shown that REEP6 is essential for male fertility, as it has a critical role in sperm motility, and likely roles in annulus function and head–tail coupling. Future studies will investigate whether the phenotype of the *Reep6* KO is due to the loss of REEP6 causing aberrant motor protein movement, mislocalization of proteins essential for IMT, or intraflagellar transport [50–52], or mislocalization of essential GPCRs [53] through proteomic and immunofluorescent staining approaches.

We previously identified seven individuals from five families with autosomal recessive mutations in *REEP6* that were causative of their RP [10]. As RP is the most common inherited retinal dystrophy (affecting approximately 1 in 4000) [54], it will be valuable to investigate whether the sperm motility defects and sterility caused by loss of REEP6 reported herein has the same pathology in humans. This information could inform patients of reproductive age living with RP to help improve success in pregnancy through artificial reproductive technologies and overall quality of life.

Supplementary material

Supplementary material is available at *BIOLRE* online.

Acknowledgment

The authors would like to thank Dr Anand Swaroop for providing the REEP6 antibody and the Baylor College of Medicine Pathology & Histology Core for processing and embedding histology samples. We would also like to thank Dr Jianhua Gu and Huie Wang at Houston Methodist Research Institute's Electron Microscopy Core for their expertise in acquiring scanning and TEM images. We thank Dr Deborah A. O'Brien at the University of North Carolina School of Medicine for valuable assistance using the CASAnova program to classify sperm motility. We also thank Dr Thomas X. Garcia at Baylor College of Medicine Center for Drug Discovery and the University of Houston-Clear Lake for providing the mouse testis cDNA from PND 3 to 35.

Conflict of interest

The authors have declared that no conflict of interest exists.

References

1. Kumar N, Singh AK. Trends of male factor infertility, an important cause of infertility: a review of literature. *J Hum Reprod Sci* 2015; **8**:191–196.
2. Cao X, Cui Y, Zhang X, Lou J, Zhou J, Bei H, Wei R. Proteomic profile of human spermatozoa in healthy and asthenozoospermic individuals. *Reprod Biol Endocrinol* 2018; **16**:4–11.
3. Tosti E, Ménézo Y. Gamete activation: basic knowledge and clinical applications. *Hum Reprod Update* 2016; **22**:420–439.
4. Lehti MS, Sironen A. Formation and function of sperm tail structures in association with sperm motility defects. *Biol Reprod* 2017; **97**:522–536.
5. Shang Y, Zhu F, Wang L, Ouyang YC, Dong MZ, Liu C, Zhao H, Cui X, Ma D, Zhang Z, Yang X, Guo Y et al. Essential role for SUN5 in anchoring sperm head to the tail. *elife* 2017; **6**:1–19.
6. Castaneda JM, Hua R, Miyata H, Oji A, Guo Y, Cheng Y, Zhou T, Guo X, Cui Y, Shen B, Wang Z, Hu Z et al. TCTE1 is a conserved component of the dynein regulatory complex and is required for motility and metabolism in mouse spermatozoa. *Proc Natl Acad Sci USA* 2017; **114**:E5370–E5378.
7. Liu M, Ru Y, Gu Y, Tang J, Zhang T, Wu J, Yu F, Yuan Y, Xu C, Wang J, Shi H. Disruption of Ssp411 causes impaired sperm head formation and male sterility in mice. *Biochim Biophys Acta, Gen Subj* 2018; **1862**:660–668.
8. Dong FN, Amiri-Yekta A, Martinez G, Saut A, Tek J, Stouvenel L, Lorès P, Karaouzène T, Thierry-Mieg N, Satre V, Brouillet S, Daneshipour A et al. Absence of CFAP69 causes male infertility due to multiple morphological abnormalities of the flagella in human and mouse. *Am J Hum Genet* 2018; **102**:636–648.
9. Agrawal SA, Burgoyne T, Eblimit A, Bellingham J, Parfitt DA, Lane A, Nichols R, Asomugha C, Hayes MJ, Munro PM, Xu M, Wang K et al. REEP6 deficiency leads to retinal degeneration through disruption of ER homeostasis and protein trafficking. *Hum Mol Genet* 2017; **26**:2667–2677.
10. Arno G, Agrawal SA, Eblimit A, Bellingham J, Xu M, Wang F, Chakarova C, Parfitt DA, Lane A, Burgoyne T, Hull S, Carss KJ et al. Mutations in REEP6 cause autosomal-recessive retinitis pigmentosa. *Am J Hum Genet* 2016; **99**:1305–1315.
11. Björk S, Hurt CM, Ho VK, Angelotti T. REEPs are membrane shaping adapter proteins that modulate specific G protein-coupled receptor trafficking by affecting ER cargo capacity. *PLoS One* 2013; **8**:1–28.
12. Hao H, Veleri S, Sun B, Kim DS, Keeley PW, Kim JW, Yang HJ, Yadav SP, Manjunath SH, Sood R, Liu P, Reese BE et al. Regulation of a novel isoform of receptor expression enhancing protein REEP6 in rod photoreceptors by bZIP transcription factor NRL. *Hum Mol Genet* 2014; **23**:4260–4271.
13. Keeley PW, Luna G, Fariss RN, Skyles KA, Madsen NR, Raven MA, Poché RA, Swindell EC, Jamrich M, Oh EC, Swaroop A, Fisher SK et al. Development and plasticity of outer retinal circuitry following genetic removal of horizontal cells. *J Neurosci* 2013; **33**:17847–17862.
14. Mainland J, Matsunami H. Ramp like proteins RTP and REEP family of proteins. *Adv Exp Med Biol* 2012; **744**:75–86.
15. Park CR, You DJ, Park S, Mander S, Jang DE, Yeom SC, Oh SH, Ahn C, Lee SH, Seong JY, Hwang JI. The accessory proteins REEP5 and REEP6 refine CXCR1-mediated cellular responses and lung cancer progression. *Sci Rep* 2016; **6**:1–13.
16. Shibata Y, Hu J, Kozlov MM, Rapoport TA. Mechanisms shaping the membranes of cellular organelles. *Annu Rev Cell Dev Biol* 2009; **25**:329–354.
17. Sato H, Tomita H, Nakazawa T, Wakana S, Tamai M. Deleted in polyposis 1-like 1 gene (Dp1l1): a novel gene richly expressed in retinal ganglion cells. *Invest Ophthalmol Vis Sci* 2005; **46**:791–796.
18. Bellvé AR, Cavicchia JC, Millette CF, O'Brien DA, Bhatnagar YM, Dym M. Spermatogenic cells of the prepuberal mouse. Isolation and morphological characterization. *J Cell Biol* 1977; **74**:68–85.
19. Ahmed EA, de Rooij DG. Staging of mouse seminiferous tubule cross-sections. *Methods Mol Biol* 2009; **558**:263–277.
20. Quinn P, Kerin JF, Warnes GM. Improved pregnancy rate in human in vitro fertilization with the use of a medium based on the composition of human tubal fluid. *Fertil Steril* 1985; **44**:493–498.
21. Goodson SG, Zhang Z, Tsuruta JK, Wang W, O'Brien DA. Classification of mouse sperm motility patterns using an automated multiclass support vector machines model. *Biol Reprod* 2011; **84**:1207–1215.
22. Garner DL, Johnson LA. Viability assessment of mammalian sperm using SYBR-14 and propidium iodide. *Biol Reprod* 1995; **53**:276–284.
23. Pérez-Crespo M, Pintado B, Gutiérrez-Adán A. Scrotal heat stress effects on sperm viability, sperm DNA integrity, and the offspring sex ratio in mice. *Mol Reprod Dev* 2008; **75**:40–47.
24. Sutovsky P. Visualization of sperm accessory structures in the mammalian spermatids, spermatozoa, and zygotes by immunofluorescence, confocal, and immunoelectron microscopy. *Methods Mol Biol* 2004; **253**:59–77.
25. Schneider CA, Rasband WS, Eliceiri KW. NIH image to ImageJ: 25 years of image analysis. *Nat Methods* 2012; **9**:671–675.
26. Tokuhiro K, Ikawa M, Benham AM, Okabe M. Protein disulfide isomerase homolog PDILT is required for quality control of sperm membrane protein ADAM3 and male fertility [corrected]. *Proc Natl Acad Sci USA* 2012; **109**:3850–3855.
27. Lin Y-N, Roy A, Yan W, Burns KH, Matzuk MM. Loss of zona pellucida binding proteins in the acrosomal matrix disrupts acrosome biogenesis and sperm morphogenesis. *Mol Cell Biol* 2007; **27**:6794–6805.
28. Toyoda Y, Yokoyama M. The early history of the TYH medium for in vitro fertilization of mouse ova. *J Mamm Ova Res* 2018; **35**:71–71.
29. Jin M, Fujiwara E, Kakiuchi Y, Okabe M, Satouh Y, Baba SA, Chiba K, Hirohashi N. Most fertilizing mouse spermatozoa begin their acrosome reaction before contact with the zona pellucida during in vitro fertilization. *Proc Natl Acad Sci USA* 2011; **108**:4892–4896.
30. De Grava KW, Klinefelter GR. Interpreting histopathology in the epididymis. *Spermatogenesis* 2014; **4**:e979114.
31. Visconti PE, Bailey JL, Moore GD, Pan D, Olds-Clarke P, Kopf GS. Capacitation of mouse spermatozoa. I. Correlation between the capacitation state and protein tyrosine phosphorylation. *Development* 1995; **121**:1129–1137.
32. Salicioni AM, Platt MD, Wertheimer EV, Arcelay E, Allaire A, Sosnik J, Visconti PE. Signalling pathways involved in sperm capacitation. *Soc Reprod Fertil Suppl* 2007; **65**:245–259.
33. Sebkova N, Cerna M, Ded L, Peknicova J, Dvorakova-Hortova K. The slower the better: how sperm capacitation and acrosome reaction is modified in the presence of estrogens. *Reproduction* 2012; **143**:297–307.
34. Visconti PE. Understanding the molecular basis of sperm capacitation through kinase design. *Proc Natl Acad Sci USA* 2009; **106**:667–668.
35. Sloter E, Schmid TE, Marchetti F, Eskenazi B, Nath J, Wyrobek AJ. Quantitative effects of male age on sperm motion. *Hum Reprod* 2006; **21**:2868–2875.
36. Nakata H, Wakayama T, Takai Y, Iseki S. Quantitative analysis of the cellular composition in seminiferous tubules in normal and genetically modified infertile mice. *J Histochem Cytochem* 2015; **63**:99–113.
37. Bhagwat S, Dalvi V, Chandrasekhar D, Matthew T, Acharya K, Gajbhiye R, Kulkarni V, Sonawane S, Ghosalkar M, Parte P. Acetylated α-tubulin is reduced in individuals with poor sperm motility. *Fertil Steril* 2014; **101**:95–104.e3.
38. Russell LD, Ettlin RA, Sinha Hikim AP, Clegg ED. *Histological and Histopathological Evaluation of the Testis*, 1st ed. Clearwater, FL: Cache River Press; 1990.
39. O'Donnell L, O'Bryan MK. Microtubules and spermatogenesis. *Semin Cell Dev Biol* 2014; **30**:45–54.
40. Wei YL, Yang WX. The acroframosome-acroplaxome-manchette axis may function in sperm head shaping and male fertility. *Gene* 2018; **660**:28–40.
41. Guo JH, Huang Q, Studholme DJ, Wu CQ, Zhao SY. Transcriptomic analyses support the similarity of gene expression between brain and testis in human as well as mouse. *Cytogenet Genome Res* 2005; **111**:107–109.

42. Meistrich ML, Hess RA. *Assessment of Spermatogenesis Through Staging of Seminiferous Tubules*, vol. **927**. Totowa, NJ: Humana Press; 2013.
43. O'Donnell L. Mechanisms of spermiogenesis and spermiation and how they are disturbed. *Spermatogenesis* 2014; **4**:e979623.
44. Creasy D, Bube A, de Rijk E, Kandori H, Kuwahara M, Masson R, Nolte T, Reams R, Regan K, Rehm S, Rogerson P, Whitney K. Proliferative and nonproliferative lesions of the rat and mouse male reproductive system. *Toxicol Pathol* 2012; **40**:40S–121S.
45. Qian X, Wang L, Zheng B, Shi Z-M, Ge X, Jiang C-F, Qian Y-C, Li D-M, Li W, Liu X, Yin Y, Zheng J-T et al. Deficiency of Mkrn2 causes abnormal spermiogenesis and spermiation, and impairs male fertility. *Sci Rep* 2016; **6**:39318.
46. Kissel H, Georgescu MM, Larisch S, Manova K, Hunnicutt GR, Steller H. The Sept4 septin locus is required for sperm terminal differentiation in mice. *Dev Cell* 2005; **8**:353–364.
47. Kuo YC, Shen YR, Chen HI, Lin YH, Wang YY, Chen YR, Wang CY, Kuo PL. SEPT12 orchestrates the formation of mammalian sperm annulus by organizing core octameric complexes with other SEPT proteins. *J Cell Sci* 2015; **128**:923–934.
48. Moretti E, Collodel G, Mazzi L, Russo I, Giurisato E. Ultrastructural study of spermatogenesis in KSR2 deficient mice. *Transgenic Res* 2015; **24**:741–751.
49. Bower R, Tritschler D, Vanderwaal K, Perrone CA, Mueller J, Fox L, Sale WS, Porter ME. The N-DRC forms a conserved biochemical complex that maintains outer doublet alignment and limits microtubule sliding in motile axonemes. *Mol Biol Cell* 2013; **24**: 1134–1152.
50. Toshimori K, Ito C. Formation and organization of the mammalian sperm head. *Arch Histol Cytol* 2003; **66**:383–396.
51. Kierszenbaum AL, Rivkin E, Tres LL, Yoder BK, Haycraft CJ, Bornens M, Rios RM. GMAP210 and IFT88 are present in the spermatid golgi apparatus and participate in the development of the acrosome-acroplaxome complex, head-tail coupling apparatus and tail. *Dev Dyn* 2011; **240**:723–736.
52. San Agustin JT, Pazour GJ, Witman GB. Intraflagellar transport is essential for mammalian spermiogenesis but is absent in mature sperm. *Mol Biol Cell* 2015; **26**:4358–4372.
53. Flegel C, Vogel F, Hofreuter A, Wojcik S, Schoeder C, Kieć-Kononowicz K, Brockmeyer NH, Müller CE, Becker C, Altmüller J, Hatt H, Gisselmann G. Characterization of non-olfactory GPCRs in human sperm with a focus on GPR18. *Sci Rep* 2016; **6**:1–10.
54. Ferrari S, Di Iorio E, Barbaro V, Ponzin D, Sorrentino FS, Parmeggiani F. Retinitis pigmentosa: genes and disease mechanisms. *Curr Genomics* 2011; **12**:238–249.